Imprinting knots in a spinor Bose-Einstein condensate via a Raman process without knotted optical fields

Zekai Chen, * Elisha Haber, and Nicholas P. Bigelow

Department of Physics and Astronomy, University of Rochester, Rochester, New York 14627, USA and Center for Coherence and Quantum Optics, University of Rochester, Rochester, New York 14627, USA

(Received 17 May 2022; accepted 20 October 2022; published 15 November 2022)

We propose a dynamical imprinting scheme to create nodal lines of torus and lemniscate knots via a Raman process in a dilute spinor Bose-Einstein condensate. We calculate the desired parameters and the necessary spatial profiles of the Raman laser fields that couple a realistic multilevel atomic system, and demonstrate the imprinting results via a numerical calculation. Additionally, we show the capability of our method to adjust the size and the aspect ratio of the knotted nodal lines by tuning the parameters of Raman lasers that propagate along different directions.

DOI: 10.1103/PhysRevResearch.4.043109

I. INTRODUCTION

Topological structure such as vortices and knots appear in a variety of systems, including superfluid Helium [1,2], ultracold atom [3–5], condensed matter [6,7], fluid dynamical [8], and biological macromolecules such as DNA and protein [9–12]. Understanding the behavior of a system with knotted and linked topological structures can greatly extend our knowledge in many research fields such as hydrodynamics, condensed matter physics, cosmology, biology, and chemistry.

Specifically, the study of knotted optical fields draws extensive interest for its applications in quantum information [13]. Many ways of creating knots in optical systems have been demonstrated both theoretically and experimentally [13–17]. On the other hand, in recent years, ultracold spinor quantum gases have become an ideal playground for studying topological defects in superfluids given the convenience of creating vortices, 2D skyrmions, 3D skyrmions, and knotted structures in these systems [18–25]. The study of knots and topological defects in optical systems evokes a great interest in creating the topological defects of knots in the quantum gas and study their interaction and the evolution processes. There are some protocols for creating knotted structures in a spinor Bose-Einstein condensate (BEC) via engineering the laser fields in a Λ or a tripod system [25–27], yet the implementation in a multilevel atomic system demands more exploration.

In this paper, we propose a method to imprint a nodal line of knots in a pseudospin-1/2 BEC via a Raman process. With our method, the knotted nodal line structure is carried, not by the laser fields, but by the resulting effective magnetic field

Published by the American Physical Society under the terms of the Creative Commons Attribution 4.0 International license. Further distribution of this work must maintain attribution to the author(s) and the published article's title, journal citation, and DOI.

induced by the Raman process. We theoretically construct the desired structured laser fields, show the results after the imprinting process, and discuss how the desired knotted structure could be measured in a realistic system. In our protocol, the Raman lasers propagate along two orthogonal directions, which enables us to adjust the size and the aspect ratio of the imprinted nodal line.

II. THEORETICAL FORMALISM

A knot is a closed loop embedded in a three-dimensional Euclidean space \mathbb{R}^3 . Mathematically, there are many methods to construct knots and links. In this paper, we are specifically interested in the construction of torus and lemniscate knots.

Consider constructing two complex fields, $u = (r^2 -$ 1 + 2iz)/($r^2 + 1$) and $v = 2(x + iy)/(r^2 + 1)$, which satisfy $|u|^2 + |v|^2 = 1$, where $r = \sqrt{x^2 + y^2 + z^2}$. With Brauner's method [14,16,28], a complex torus knotted field can be constructed by the map

$$K(p,q) = u^p - v^q, \tag{1}$$

where p and q are positive integers. With the definition of u =u(x, y, z) and v = v(x, y, z), we constructed a map from \mathbb{R}^3 to \mathcal{C}^2 (or S^3). Then, with Brauner's method, we used the complex polynomial field K(p, q) as a map from C^2 , defined by u and v, to \mathcal{C} . Therefore, we have the map $K(p,q): \mathcal{R}^3 \to \mathcal{C}^2 \to \mathcal{C}$, where the preimage of the complex field K(p, q) in the threedimensional Euclidean space \mathbb{R}^3 has a closed nodal line with the structure of a (p, q) knot or link.

Beyond the torus knot, using the same definition of two complex fields u and v, one can also construct a map to a lemniscate knot. Specifically, for a pigtail knot [14,16], the map takes the form

$$K(n) = 64u^{3} - 12u(2v^{n} - 2v^{*n} + 3)$$
$$- (14v^{n} + 14v^{*n} + v^{2n} - v^{*2n}),$$
(2)

where n is a positive integer.

^{*}Current address: Institut für Experimentalphysik und Zentrum für Quantenphysik, Universität Innsbruck, 6020 Innsbruck, Austria. †nicholas.bigelow@rochester.edu

III. IMPRINTING SCHEME VIA A RAMAN PROCESS

Our goal is to imprint the knotted complex field, K(x, y, z), onto the wave function of a Bose-Einstein condensate. One straightforward approach is to engineer the electromagnetic field that interacts with the atoms such that the topological structure carried by the fields is transferred to the wave function of the BEC.

The discussion in the last section shows that one can construct a complex field, K(x, y, z), from two complex fields, u(x, y, z) and v(x, y, z), so that the singular points of |K(x, y, z)| in \mathbb{R}^3 form a knot. We consider using a Raman process to imprint the knotted structure onto the wave function of a pseudospin-1/2 BEC, where the atom-field coupling can generally be written as a two-level Hamiltonian of the form

$$H_R = \hbar(\Omega_d \hat{\mathbb{1}} + \Omega_3 \hat{\sigma}_3 + \Omega_K \hat{\sigma}_+ + \Omega_K^* \hat{\sigma}_-), \tag{3}$$

where $\hbar\Omega_d$ is an energy offset, Ω_K is a knotted complex field, Ω_3 is the z component of the two-photon Rabi frequency, and the total two-photon Rabi frequency is defined as $\Omega = \sqrt{|\Omega_K|^2 + |\Omega_3|^2}$. $\hat{\sigma}_3$ and $\hat{\sigma}_\pm = \hat{\sigma}_1 \pm i\hat{\sigma}_2$ are Pauli matrices and $\hat{\mathbb{I}}$ is the identity matrix. We can neglect the energy offset $\hbar\Omega_d$ as it only sets the global phase of the wave function. The evolution operator corresponding to the Raman Hamiltonian given by Eq. (3) takes the form

$$U(t) = \begin{pmatrix} \cos \gamma - i \frac{\Omega_3}{\Omega} \sin \gamma & -i \frac{\Omega_K}{\Omega} \sin \gamma \\ -i \frac{\Omega_K^*}{\Omega} \sin \gamma & \cos \gamma + i \frac{\Omega_3}{\Omega} \sin \gamma \end{pmatrix}, \quad (4)$$

where $\gamma = \Omega t/2$. If we apply U(t) to the spin up state, $\xi_0 = (1, 0)^T$, where ξ_0 is the dimensionless spinor part of the order parameter of the BEC at t = 0, then we get

$$\xi_t = \begin{pmatrix} \cos \gamma - i \frac{\Omega_3}{\Omega} \sin \gamma \\ -i \frac{\Omega_K}{\Omega} \sin \gamma \end{pmatrix}. \tag{5}$$

Equation (5) shows that if we let $\Omega_K \propto K$, then the singular points of the spin down component of ξ_t will be the same as the singular points in Ω_K . Therefore, the knotted singular structure will be imprinted on the wave function of the pseudospin-1/2 BEC.

The complex fields K(p,q) in Eq. (1) and K(n) in Eq. (2) take the form of complex polynomials that consist of different orders of fractions of the complex variables u and v. However, it is not easy to use paraxial polynomial laser beams to achieve such complex fields in the laboratory. Therefore, similar to the approach used to generate knotted nodal lines in the optical fields, we apply the technique known as "overhomogenization" [16,29], which is the process of multiplying the complex polynomials with the lowest power of $1 + r^2$ to make sure that there is no common factor of $1 + r^2$ in the complex polynomial after we get rid of the denominator, while preserving the knotted structure. We then normalize the polynomial Raman laser beams by Gaussian profiles. The resulting normalized field, $\tilde{K} = K(1 + r^2)^s$, where s is a positive integer, carries the desired nodal structure.

To imprint a trefoil knot, we take p = 2, q = 3, and n = 3. The normalized field after overhomogenization is K(2, 3) = $(u^2 - v^3)(1 + r^2)^3$, and the complex field $\Omega_{\tilde{K}}$ is given by

$$\Omega_{\tilde{K}}^{\text{trefoil}} = \Omega_0 [\tilde{\rho}^6 - \tilde{\rho}^4 - \tilde{\rho}^2 - 8\tilde{\rho}^3 e^{i3\phi}
+ \tilde{z}^6 + 4i\tilde{z}^5 - 5\tilde{z}^4 - 5\tilde{z}^2 - 4i\tilde{z} + 1
+ \tilde{\rho}^2 (3\tilde{z}^4 + 8i\tilde{z}^3 - 6\tilde{z}^2) + \tilde{\rho}^4 (3\tilde{z}^2 + 4i\tilde{z})], (6)$$

where Ω_0 is the amplitude of the complex field, and

$$\tilde{\rho} = \rho/w_t,$$

$$\tilde{z} = z/w_z,$$
(7)

where $\rho = \sqrt{x^2 + y^2}$, and w_t and w_z are two scaling factors that can be used to control the size and aspect ratio of the topological structure we imprint onto the BEC.

For a lemniscate knot, such as a figure-8 knot, we take n=4. The normalized field after overhomogenization is $K=(64u^3-12u(2v^p-2v^{*p}+3)-(14v^p+14v^{*p}+v^{2p}-v^{*2p}))(1+r^2)^4$, and the complex field, $\Omega_{\tilde{K}}$, takes the form

$$\Omega_{\tilde{K}}^{\text{fig}-8} = 4\Omega_0 \{ 16(1 + \tilde{z}^2 + \tilde{\rho}^2) [(i + \tilde{z})^2 + \tilde{\rho}^2]^3
- 28\tilde{\rho}^2 (1 + \tilde{z}^2 + \tilde{\rho}^2)^2 \cos 2\phi
- 3(1 + \tilde{z}^2 + \tilde{\rho}^2) [(i + \tilde{z})^2 + \tilde{\rho}^2] [3(1 + \tilde{z}^2 + \tilde{\rho}^2)^2
+ 8i\tilde{\rho}^2 \sin 2\phi] - 8i\tilde{\rho}^4 \sin 4\phi \}.$$
(8)

It is mathematically rigorous that Eq. (8) carries a figure-8 knotted structure as a closed contour formed by its complex roots. However, in practice, one can also adjust some of the coefficients in the expansion form of the knotted complex field $\Omega_{\tilde{K}}$ to engineer the shape and scale of the knot [13,15,17]. In our calculation results, we roughly optimize the shape of imprinted figure-8 knot by changing some of the coefficients in the expansion form of $\Omega_{\tilde{K}}^{\text{fig-8}}$, and the resulting field becomes $\Omega_{\tilde{K}}^{\text{fig-8'}}$ which is given by Eq. (A2) in the Appendix

 $\Omega_{\tilde{K}}^{\text{fig-8'}}$, which is given by Eq. (A2) in the Appendix. If we regard the spin up and down components of the wave function as analogous to the left and right circular polarization components of optical fields, then the contour formed by the singular points in the pseudospin-1/2 BEC order parameter can be regarded as a knotted nodal line (C line) [13]. For a real C line produced in optical fields, auxiliary fields with different polarization are required to satisfy Maxwell's equations and avoid reconnection of the nodal line. The imprinting scheme of a nodal line in a BEC does not require auxiliary optical fields, and none of the Raman fields carry the entire knotted field. Instead, it is the off-diagonal matrix elements in Eq. (3) that carry the desired topological structure. Therefore, for experimental convenience, structured paraxial beams propagating along orthogonal axes can be used to generate the Raman fields.

IV. CALCULATION RESULTS

A. Imprinting trefoil and figure-8 knots

Our imprinting scheme starts from a dilute pseudospin-1/2 BEC in a shallow, isotropic harmonic trap with all atoms initially in the spin up state. Then, the Raman laser pulse is applied nonadiabatically to let the system evolve with evolution operator U(t) in Eq. (4), which carries the knotted nodal line structure in the Ω_K term. We numerically demonstrate

the imprinting of a trefoil and figure-8 knot, as examples of torus and lemniscate knots, respectively. Using multiple Raman laser fields, we can construct the complex fields for both knots, which are given in Eqs. (6) and (8). We consider a rapid imprinting process with an imprinting pulse length τ_p of around $10-80~\mu s$, which allows us to neglect the effects of kinetic energy and atomic interactions on the BEC dynamics.

In practice, one can measure the Stokes parameters to fully reconstruct the order parameter of a pseudospin-1/2 BEC. The Stokes parameters of a spin-1/2 order parameter, $\xi = (\xi_1, \xi_2)^T$, take the form

$$s_{1} = \xi_{1}\xi_{2}^{*} + \xi_{1}^{*}\xi_{2},$$

$$s_{2} = -i(\xi_{1}\xi_{2}^{*} - \xi_{1}^{*}\xi_{2}),$$

$$s_{3} = |\xi_{1}|^{2} - |\xi_{2}|^{2}.$$
(9)

Plugging in the state given by Eq. (5), we get the z component of the Stokes parameters,

$$s_3(t) = \cos^2 \gamma(t) + \left(1 - \frac{2|\Omega_K|^2}{|\Omega|^2}\right) \sin^2 \gamma(t).$$
 (10)

With the spatial profile of the Raman laser fields and the chosen parameters, the power of the laser fields at the center regime where the knotted effective magnetic field exists is very low. Therefore, the population transfer between the spin up and spin down states is small. To capture the nodal line structure imprinted in the pseudospin-1/2 BEC wave function, we calculated the logarithm of $1-s_3$, which takes the form

$$\log_{10}(1 - s_3) = \log_{10} 2 + 2\log_{10} |\Omega_K|$$

$$-2\log_{10} \Omega + \log_{10} [\sin^2 \gamma].$$
 (11)

Equation (11) diverges at the nodal line given by $\Omega_K = 0$. Therefore, one can capture the nodal line structure in the BEC wave function by measuring the Stokes parameters. At points in the neighborhood of $\gamma = k\pi$, where k is a positive integer, the last term in Eq. (11) takes a very large value. This makes it hard to distinguish these points from the knotted nodal line structure in the map of $\log_{10}(1-s_3)$. Although the knotted nodal line is present in the BEC after each realization, the last term in Eq. (11) can make it hard to observe the knotted structure using the same approach we used to observe the trefoil knot, as Eq. (11) diverges at the nodal line given by $\Omega_K = 0$. To get around the problem, one can vary the imprinting pulse length, τ_p , and average the results. Eq. (11) will then by given by

$$\begin{aligned} \log_{10}(1 - \bar{s}_3) &= \log_{10} 2 + 2\log_{10} |\Omega_K| \\ &- 2\log_{10} \Omega + \log_{10} [\overline{\sin^2 \gamma}], \end{aligned} (12)$$

where \bar{s}_3 is the averaged s_3 , $\overline{\sin^2 \gamma} = \frac{1}{N} \sum_{i=1}^N \sin^2 \gamma(t_i)$, and N denotes the number of measurements. After averaging the results with different pulse lengths, the influence of the last term in Eq. (12) becomes negligible, and $\log_{10} (1 - \bar{s}_3)$ will only diverge at the nodal line.

We can construct the complex field for a trefoil knot, given by Eq. (6), using the Raman laser fields given by Eq. (A1) in the Appendix, by following the imprinting scheme described above. The calculation results are shown in Fig. 1. In Fig. 1, the calculation results of the imprinting of a trefoil knot with the nodal line along with the horizontal and vertical cuts of $\log_{10}(1-s_3)$ and corresponding phase maps are shown. For the imprinting process, we apply a single Raman laser pulse with duration $\tau_p = 10~\mu s$. The one-photon Rabi frequencies of the four pairs of Raman lasers are given in the Appendix.

We find the imprinting process of a figure-8 knot numerically more difficult than imprinting the trefoil knot. The imprinted figure-8 knot that results from the complex field $\Omega_{\tilde{K}}^{fig-8}$, given by Eq. (8), has a poor shape. By changing some of the coefficients in the expanded form of $\Omega_{\tilde{K}}^{fig-8}$, we obtain a complex field $\Omega_{\tilde{K}}^{fig-8'}$ given by Eq. (A2), that results in a better figure-8 knot. The necessary Raman fields are given by Eq. (A3) in the Appendix. The calculated imprinting results are shown in Fig. 2. For the figure-8 knot, the intensity of the Raman laser fields varies drastically between the center regime of the knot and the outer region. Consequently, the amplitude of the knotted off-diagonal matrix element $|\Omega_K|$ in Eq. (3) varies drastically as well.

We applied 40 pulses with pulse lengths ranging from $\tau_p=40~\mu s$ to 80 μs to numerically capture the knotted structure in the same way as the trefoil knot, and we averaged the results to clean out the undesired nonsingular structure surrounding the nodal line [see Eq. (12)]. This was necessary due to the drastic variance in the amplitude of the Raman laser fields. The calculation results are shown in Fig. 2. In Fig. 2, we show the nodal line extracted from the Stokes parameters after the imprinting pulse from different angle of view along with the corresponding horizontal and vertical cuts of $\log_{10}(1-\bar{s}_3)$. In total, we propose using 9 pairs of Raman lasers for imprinting the figure-8 knot, and the corresponding one-photon Rabi frequencies are given in the Appendix.

For both Figs. 1 and 2, the beam waist of the Gaussian envelope was set to be $w_0 = 10 \, \mu m$, and the scaling factors were chosen to be $w_t = w_r = 5 \, \mu m$. With these parameters, we can ignore the effects caused by the Gouy phase and nonlinear propagation phase as the Rayleigh range is much larger than the region of interest. Additionally, we point out that the pulse lengths, τ_p , were not optimized. In fact, it is hard to define an optimized pulse duration in such cases, since the two-photon Rabi frequency in Raman pulses with structured fields is spatially varying. Therefore, we picked pulse lengths that were sufficient for us to show the desired nodal line structure, and demonstrated that by applying pulses using multiple Raman laser fields with carefully engineered spatial modes and amplitudes, we could imprint a knotted nodal line in a dilute pseudospin-1/2 BEC.

B. Controlling the size and the aspect ratio of the nodal line

In the previous subsection, we showed that by constructing structured complex fields with a Raman process, both a torus and lemniscate knot can be imprinted onto a BEC without requiring the laser fields to contain the knotted structure. By tuning the parameters w_t and w_z in Eq. (7), one can control the detailed structure of the laser fields in the radial and

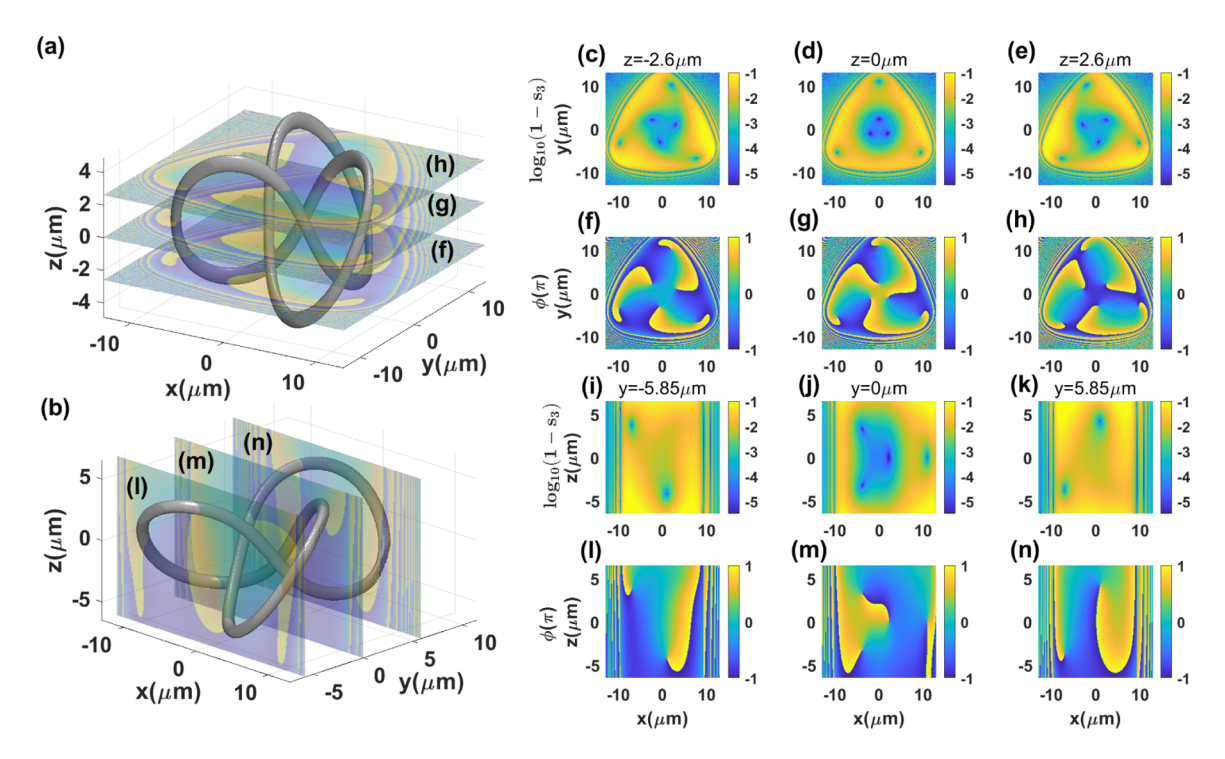


FIG. 1. Theoretical results for imprinting a trefoil knot. In [(a), (b)] we show the nodal line extracted from the Stokes parameters after the imprinting pulse from different angles. The semitransparent cuts are phase maps obtained from the Stokes parameters at different planes in different directions. The horizontal cuts of $\log_{10}(1-s_3)$ and the corresponding phase maps at different z planes ($z=-2.6 \, \mu m$, respectively) are shown in [(c)-(f)]. The vertical cuts of $\log_{10}(1-s_3)$ and the corresponding phase maps at different z planes ($z=-2.6 \, \mu m$, respectively) are shown in [(i)-(n)]. The phase maps [(f)-(h)] and [(l)-(n)] correspond to the semitransparent cuts in (a) and (b), respectively.

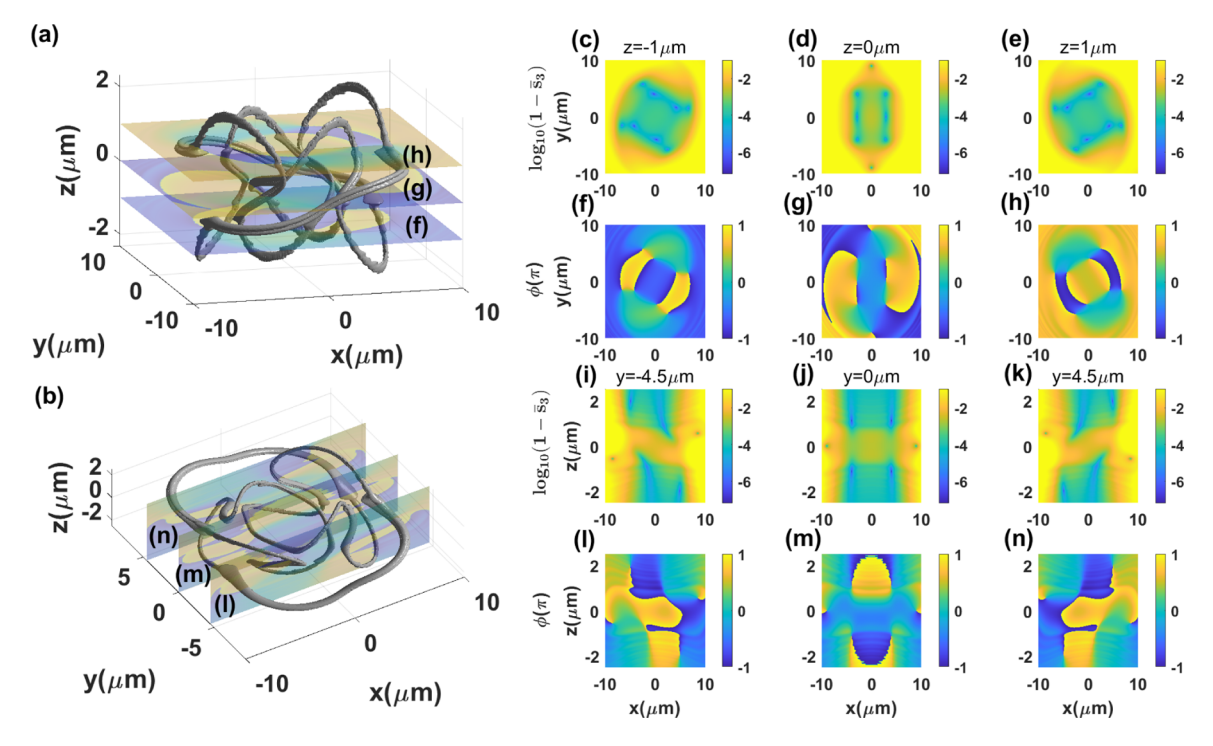


FIG. 2. Theoretical results for imprinting a figure-8 knot. In [(a), (b)] we show the nodal line extracted from the Stokes parameters after the imprinting pulse from different angles. The semitransparent cuts are phase maps obtained from the Stokes parameters at different planes in different directions. The horizontal cuts of $\log_{10}(1-\bar{s}_3)$ and the corresponding phase maps at different z planes (z=-1 μm , z=0 μm , and z=1 μm , respectively) are shown in [(c)–(f)]. The vertical cuts of $\log_{10}(1-\bar{s}_3)$ and the corresponding phase maps at different y planes (y=-4.5 μm , y=0 μm , and y=4.5 μm , respectively) are shown in [(i)–(n)]. The phase maps [(f)–(h)] and [(l)–(n)] correspond to the semitransparent cuts in (a) and (b), respectively.

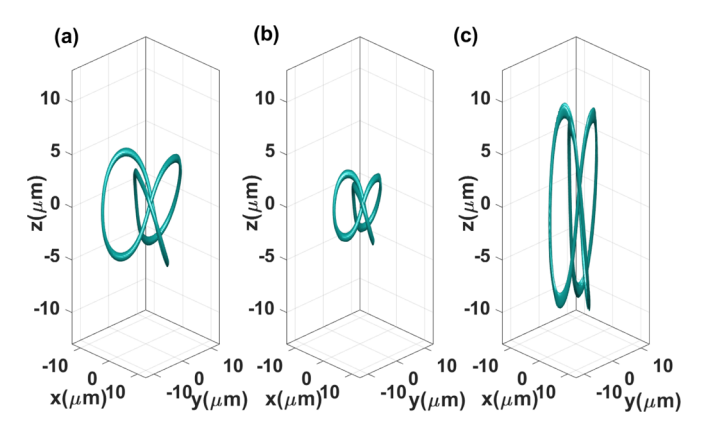


FIG. 3. Control over the size and aspect ratio of the knot. Here we take the trefoil knot as our example. (a) A trefoil knot with $w_t=w_z=5~\mu\mathrm{m}$ for reference. (b) A trefoil knot with a shrunken size but the same aspect ratio as (a), where $w_t=w_z=3~\mu\mathrm{m}$. (c) A trefoil knot with a different aspect ratio, where $w_t=3~\mu\mathrm{m}$, and $w_z=10~\mu\mathrm{m}$. We take $w_0=10~\mu\mathrm{m}$ for all three cases.

longitudinal directions separately, and thus independently vary the size and the aspect ratio of the knotted nodal line.

We use the trefoil knot as our example, in Fig. 3 we demonstrated control over the size and the aspect ratio of the knotted structure. We show that by tuning the scaling parameters w_t and w_z , our method is capable of changing the size and the aspect ratio of the knotted nodal line imprinted on the BEC independently, which can provide more freedom in when studying the evolution of the knotted BEC experimentally.

V. EXPERIMENTAL IMPLEMENTATION

In our imprinting scheme, the knotted nodal line is embedded in the effective magnetic field generated by the Raman process. To create the desired off-diagonal matrix elements [given by Eqs. (6) and (8)] in the effective two-level Hamiltonian [given by Eq. (3)], multiple Raman beams are needed. There are many potential ways to engineer the Raman beams to achieve the desired effective magnetic field [26,27], and here we only describe our example in detail.

In this paper, we choose 87 Rb to be our atomic system, where the Raman process couples two Zeeman sublevels in the $5S_{\frac{1}{2}}$, F=1 hyperfine ground state manifold. The semiclassical atom-laser interaction Hamiltonian can be described using second-order perturbation theory [30,31], and for the Raman process shown in Fig. 4, the resulting effective Hamiltonian acting on the F=1 ground-state manifold takes the form

$$H = \sum_{\alpha,F,m_F} \left[\frac{\left(c_{m_F,m_F}^{\mathcal{F}}\right)^2}{\Delta_{\alpha,m_F,m_F}^{\mathcal{F}}} |\Omega_{\alpha}|^2 + \delta_{m_F} \right] |m_F\rangle\langle m_F|$$

$$+ \sum_{\alpha,\beta,F,m_F} \frac{1}{2} \left(\frac{1}{\Delta_{\alpha,m_F,m_F+1}^{\mathcal{F}}} + \frac{1}{\Delta_{\beta,m_F,m_F-1}^{\mathcal{F}}} \right)$$

$$\times c_{m_F,m_F+1}^{\mathcal{F}} c_{m_F,m_F-1}^{\mathcal{F}}$$

$$\times \Omega_{\alpha}^{\mathcal{F}} \Omega_{\beta} |m_F\rangle\langle m_F + 1| + \text{H.c.}, \tag{13}$$

where $\alpha, \beta = a, b, c, \ldots, r$ denote different Raman laser fields, $m_F = \mp 1$ denotes $|F = 1, m_F = \mp 1\rangle$ states on the $5S_{\frac{1}{2}}, F = 1$ ground-state manifold. $\mathcal{F} = 1, 2$ denotes the

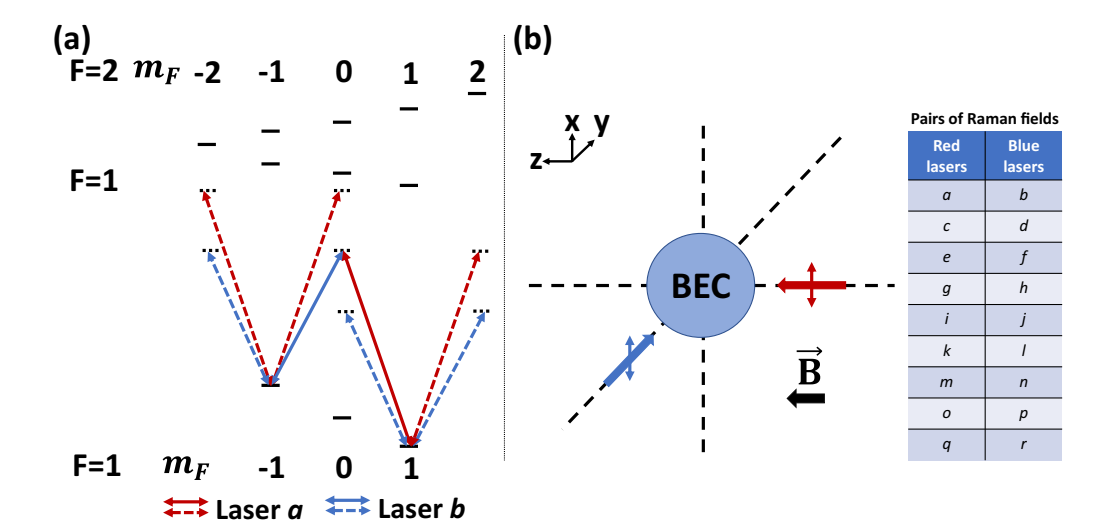


FIG. 4. (a) Level diagram of the Raman process that we consider in a 87 Rb system. All Raman fields are grouped into red and blue lasers, where members of the same group differ only in their wavelengths. Each red and blue laser is paired with a laser from the other group, and each pair realizes a two-photon resonance (lasers a and b are shown in the figure as an example, and the solid arrows indicate a resonance). The one-photon detunings for each pair were chosen so that the two-photon Raman coupling between different pairs would be negligible (see the Appendix). (b) Laser configuration of the Raman process. The laser colors are the same as (a), both of their polarizations are linear polarization along x axis, as indicated by the small arrows. In both (a) and (b), red lasers are Raman lasers propagating along the +z direction, and blue lasers are Raman lasers propagating along the +z direction. Four pairs of lasers (lasers a-b) are used to imprint the trefoil knot, and nine pairs a-b0 are used to imprint the figure-8 knot. Which Raman lasers are pairs that realize a two-photon resonance are shown in the table. The bias magnetic field is in the a-b1 direction.

 $5P_{\frac{1}{2}}, F=1$ and $5P_{\frac{1}{2}}, F=2$ manifolds, respectively. $\Omega_{\alpha}=$ $d_{D_1} \cdot \vec{E}_{\alpha}/\hbar$ is the one-photon Rabi frequency for laser $\alpha =$ a, b, c, \ldots, r , where \vec{d}_{D_1} is the electric dipole moment of the D_1 transition and \vec{E}_{α} is the electric field of the corresponding Raman laser field. $\Delta_{\alpha,m_F,m_F'}^{\mathcal{F}} = \omega_{\alpha} - (\omega_{\mathcal{F},m_{F'}}^e - \omega_{F=1,m_F}^g)$ and $\Delta_{\beta,m_F,m_F'}^{\mathcal{F}} = \omega_{\beta} - (\omega_{\mathcal{F},m_{F'}}^e - \omega_{F=1,m_F}^g)$ are one-photon detunings, where ω_{α} and ω_{β} are the angular frequencies of the Raman lasers, $\omega_{\mathcal{F},m_{F'}}^e$ and $\omega_{F=1,m_F}^g$ are the angular frequencies of the corresponding excited and ground states, δ_{m_F} is the two-photon detuning of $|F=1, m_F=0, \pm 1\rangle$ states, and $c_{m_F,m_F}^{\mathcal{F}}$ is the dipole matrix elements for certain polarization of lights of ⁸⁷Rb atom [32]. With the above definitions, all one-photon detunings and one-photon Rabi frequencies for specific couplings can be calculated from the Rabi frequencies and detunings from the D_1 transition and the hyperfine dipole matrix elements. Plugging the Raman laser fields for knot imprinting into the effective Hamiltonian in Eq. (13), and due to the fact that the Raman laser fields can be decomposed into right- and left-handed circular polarizations, as shown in Fig. 4, only $|1\rangle = |F = 1, m_F = -1\rangle$ and $|2\rangle =$ $|F=1, m_F=1\rangle$ states will be coupled, and they form the pseudospin-1/2 system that we are interested in this paper. Therefore, we can project the system to the subspace of the pseudospin-1/2 system, and write down a general effective two-level Hamiltonian for the Raman process given in Eq. (3).

To imprint the knotted nodal line onto the pseudospin-1/2 BEC, one needs to engineer the off-diagonal matrix element of Eq. (3), $\hbar\Omega_K$, properly so that the knotted nodal line is embedded in the complex field Ω_K . We propose to use multiple paired Raman lasers with different detunings, spatial profiles, and propagation directions to construct the desired knotted complex fields $\Omega_K^{\text{trefoil}}$ and $\Omega_K^{\text{fig}-8'}$. With the laser configuration shown in Fig. 4, one can engineer the detunings of the Raman fields to ensure that only the paired lasers that are shown in the table in Fig. 4 form two-photon resonances, and thus contribute to Ω_K . Different detunings of Raman lasers can be achieved using acousto-optical modulators (AOMs), and the detunings used in the calculations are given in the Appendix. The Raman coupling from the lasers that are not paired by two-photon resonances are negligible due to the rotating wave approximation.

To work out the specific profile of each Raman laser field, one can decompose the knotted complex fields $\Omega_{\tilde{K}}^{\text{trefoil}}$ and $\Omega_{\tilde{K}}^{\text{fig-8'}}$ into the sum of products of the polynomials $\tilde{\rho}$ and \tilde{z} . Then, each term in the summation corresponds to one pair of Raman lasers, one that propagates along the y axis, and one along the z axis. The profiles of each pair are given by the corresponding polynomials \tilde{z} and $\tilde{\rho}$, respectively. All of the Raman laser fields can be constructed via coherent superpositions of Gaussian, Laguerre-Gaussian, and Hermite-Gaussian beams, with beam waists denoted w_0 . Therefore, the complex field $\Omega_{\tilde{K}}$ generated from the Raman laser fields is proportional to the desired knotted complex field \tilde{K} , with a factor of $\exp\{-\frac{\rho^2+\eta^2}{2w_0^2}\}$, where $\rho=\sqrt{x^2+y^2}$ and $\eta=\sqrt{x^2+z^2}$. The Raman laser fields that we use for imprinting knotted nodal line are given in the Appendix.

One effective way to create the structured laser fields to imprint the knotted nodal lines (see the fields in the Appendix) is to use a spatial-light modulator (SLM) or digital micromirror device (DMD) [33,34]. The atomic level diagram and the laser configuration for our protocol is shown in Fig. 4. The Raman lasers are all far detuned from the $5S_{\frac{1}{2}}$, F=1 to $5P_{\frac{1}{2}}$, F=1 D_1 transition, and the one-photon Rabi frequencies and detunings from the specific D_1 transitions for the Raman laser fields for both the trefoil and figure-8 knots are also given in the Appendix.

The imprinting process could proceed as follows. First, a pseudospin-1/2 BEC with all of the population in the spin up state should be produced in an optical dipole trap. The bias magnetic field is then turned on, and the imprinting Raman lasers are nonadiabatically turned on for a pulse duration τ_p . The desired knotted nodal line structure is thus imprinted into the BEC, and to observe it one could measure the Stokes parameters of the BEC. After the imprinting pulse, $\pi/2$ spin rotation pulses can be applied to the BEC via Raman lasers [19,20,35,36] so that the different components of the Stokes parameters can be obtained by a Stern-Gerlach time-of-flight (TOF) measurement.

Additionally, it is worthwhile to point out that the different propagation directions of the Raman laser fields in our protocol do not cause a fast phase modulation along their propagation directions. With our laser configuration, the Raman process couples the state $|1, \vec{p}_1\rangle$ and $|2, \vec{p}_2\rangle$, where $\vec{p}_1 = 0$ and $\vec{p}_2 = \hbar(\vec{k}_x + \vec{k}_z)$ stand for momentum states. In the TOF image, the basis we measure in is the momentum state basis, so one will not see the phase modulation due to the momentum transfer during the Raman process [35,36]. Also, the spin rotation operation before the Stern-Gerlach TOF imaging needs to be achieved by two Gaussian Raman laser fields that have a two-photon resonance between states $|1, \vec{p}_1\rangle$ and $|2, \vec{p}_2\rangle$. For such a spin rotation Raman pulse, the Raman beams have Gaussian profiles that are broad enough so that they can be regarded as plane waves in the regime of interest. More importantly, the two spin rotation Raman lasers need to propagate along the same directions as the knot imprinting Raman lasers to ensure that they do not transfer the population to different momentum states other than the two states $|1, \vec{p}_1\rangle$ and $|2, \vec{p}_2\rangle$, otherwise there will be extra undesired momentum states in the Stern-Garlach time-of-flight measurement and mess up the interference results.

VI. CONCLUSIONS

To conclude, we proposed a protocol to imprint a nodal line of the torus and lemniscate knots in a pseudospin-1/2 Bose-Einstein condensate. With our method, the nodal line is imprinted by evolving the BEC in a knotted effective magnetic field induced by a Raman process. To engineer the effective magnetic field, we introduce multiple pairs of paraxial Raman lasers with different one-photon detunings, but no knotted laser fields. Our laser fields have different spatial modes, and propagate along two orthogonal directions. Using ⁸⁷Rb as an example system, we showed the theoretical results of imprinting a trefoil and a figure-8 knot. Additionally, we demonstrated that we can control the size and aspect ratio of the imprinted knotted nodal line by varying

the parameters of the lasers. The independent control of the Raman lasers fields that propagate along different directions makes our method more flexible to fit with different BEC systems to match the desired size, shape and aspect ratio of the BEC. Our method could be used to imprint other topological defects, such as Hopf links and pairs of vortices, with appropriately designed polynomial Raman laser fields. It also provides the opportunity to experimentally explore knotted topological excitations in a spinor Bose-Einstein condensate.

ACKNOWLEDGMENT

We thank Y. Zhou and T. Yang for useful discussions. This work is supported by NSF Grant No. PHY 1708008 and NASA/JPL RSA 1656126.

APPENDIX: CONSTRUCTION OF THE RAMAN PROCESS HAMILTONIAN

The laser fields that we consider using in the trefoil knot imprinting scheme are

$$\begin{split} \vec{E}_{a} &= E_{ab}e^{-\frac{\rho^{2}}{2w_{0}^{2}}}e^{-i(k_{a}z-\omega_{a}t)}\hat{\epsilon}_{v}, \\ \vec{E}_{b} &= E_{ab}(1-4i\tilde{z}-5\tilde{z}^{2}-5\tilde{z}^{4}+4i\tilde{z}^{5}+\tilde{z}^{6})e^{-\frac{-\eta^{2}}{2w_{0}^{2}}}e^{-i(k_{b}y-\omega_{b}t)}\hat{\epsilon}_{v}, \\ \vec{E}_{c} &= E_{cd}(\tilde{\rho}^{6}-\tilde{\rho}^{4}-\tilde{\rho}^{2}-8e^{3i\phi}\tilde{\rho}^{3})e^{-\frac{\rho^{2}}{2w_{0}^{2}}}e^{-i(k_{c}z-\omega_{c}t)}\hat{\epsilon}_{v}, \\ \vec{E}_{d} &= E_{cd}e^{-\frac{\eta^{2}}{2w_{0}^{2}}}e^{-i(k_{d}y-\omega_{d}t)}\hat{\epsilon}_{v}, \\ \vec{E}_{e} &= E_{ef}\tilde{\rho}^{2}e^{-\frac{\rho^{2}}{2w_{0}^{2}}}e^{-i(k_{e}z-\omega_{e}t)}\hat{\epsilon}_{v}, \\ \vec{E}_{f} &= E_{ef}(3\tilde{z}^{4}+8i\tilde{z}^{3}-6\tilde{z}^{2})e^{-\frac{-\eta^{2}}{2w_{0}^{2}}}e^{-i(k_{f}y-\omega_{f}t)}\hat{\epsilon}_{v}, \\ \vec{E}_{g} &= E_{gh}\tilde{\rho}^{4}e^{-\frac{\rho^{2}}{2w_{0}^{2}}}e^{-i(k_{g}z-\omega_{g}t)}\hat{\epsilon}_{v}, \\ \vec{E}_{h} &= E_{gh}(2\tilde{z}^{2}+4i\tilde{z})e^{-\frac{-\eta^{2}}{2w_{0}^{2}}}e^{-i(k_{h}y-\omega_{h}t)}\hat{\epsilon}_{v}, \end{split}$$
(A1)

where $\hat{\epsilon}_v = (\hat{\epsilon}_1 + \hat{\epsilon}_{-1})/\sqrt{2}$ is the polarization vector, $\hat{\epsilon}_{\pm 1}$ denotes the polarization vector of right or left circular polarization with respect to +z direction, k_ζ with $\zeta = a, b, \ldots, h$ are angular wave numbers for different laser fields, $\eta = \sqrt{x^2 + z^2}$, and w_0 is the beam waist of the Gaussian beam, which is considered to be much larger than the size of the BEC so that we can ignore the curvature induced by the Gaussian profile. For the figure-8 knot, as discussed in the main text, we altered some coefficients in the expanded form of the polynomial for the complex field in Eq. (8) to make the shape of the figure-8 knot better. In our calculations, we use

$$\begin{split} \Omega_{\tilde{K}}^{\text{fig}-8'} &= \Omega_0 [-28 + 312 i \tilde{z} + 968 \tilde{z}^2 - 1112 i \tilde{z}^3 - 1112 i \tilde{z}^5 - 968 \tilde{z}^6 + 312 i \tilde{z}^7 + 28 \tilde{z}^8 \\ &+ 50 \tilde{\rho}^2 - 25 \tilde{\rho}^6 + 7 \tilde{\rho}^8 - 28 \tilde{\rho}^2 \cos 2\phi - 14 \tilde{\rho}^4 \cos 2\phi - 7 \tilde{\rho}^6 \cos 2\phi + 24 i \tilde{\rho}^2 \sin 2\phi - 24 i \tilde{\rho}^6 \sin 2\phi - 8 i \tilde{\rho}^4 \sin 4\phi \\ &- \tilde{\rho}^2 (150 i \tilde{z} + 428 i \tilde{z}^3 + 534 \tilde{z}^4 - 234 i \tilde{z}^5 - 28 \tilde{z}^6) + \tilde{\rho}^2 \cos 2\phi (224 \tilde{z}^2 - 112 \tilde{z}^4) \\ &+ \tilde{\rho}^2 \sin 2\phi (192 \tilde{z} + 192 \tilde{z}^3 - 96 i \tilde{z}^4) - \tilde{\rho}^4 (600 i \tilde{z} + 1368 \tilde{z}^2 - 936 i \tilde{z}^3 - 168 \tilde{z}^4) - \tilde{\rho}^4 \cos 2\phi 224 \tilde{z}^2 \\ &+ \tilde{\rho}^4 \sin 2\phi (192 \tilde{z} - 192 i \tilde{z}^2) + \tilde{\rho}^6 (312 i \tilde{z} + 112 \tilde{z}^2)]. \end{split} \tag{A2}$$

As a result, the Raman laser fields used for constructing the complex field in Eq. (A2) are

$$\begin{split} \vec{E}_{a} &= 50E_{ab}e^{-\frac{\rho^{2}}{2w_{0}^{2}}}e^{-i(k_{a}z-\omega_{a}t)}\hat{\epsilon}_{v}, \\ \vec{E}_{b} &= E_{ab}\frac{1}{50}(-28+312i\tilde{z}+968\tilde{z}^{2}-1112i\tilde{z}^{3}-1112i\tilde{z}^{5}-968\tilde{z}^{6}+312i\tilde{z}^{7}+28\tilde{z}^{8})e^{-\frac{\eta^{2}}{2w_{0}^{2}}}e^{-i(k_{b}y-\omega_{b}t)}\hat{\epsilon}_{v}, \\ \vec{E}_{c} &= E_{cd}\frac{1}{50}(100\tilde{\rho}^{2}-25\tilde{\rho}^{6}+14\tilde{\rho}^{8}-56\tilde{\rho}^{2}\cos2\phi-28\tilde{\rho}^{4}\cos2\phi-14\tilde{\rho}^{6}\cos2\phi+48i\tilde{\rho}^{2}\sin2\phi\\ &-48i\tilde{\rho}^{6}\sin2\phi-16i\tilde{\rho}^{4}\sin4\phi)e^{-\frac{\rho^{2}}{2w_{0}^{2}}}e^{-i(k_{c}z-\omega_{c}t)}\hat{\epsilon}_{v}, \\ \vec{E}_{d} &= 25E_{cd}e^{-\frac{\eta^{2}}{2w_{0}^{2}}}e^{-i(k_{d}y-\omega_{d}t)}\hat{\epsilon}_{v}, \\ \vec{E}_{e} &= 25E_{ef}\tilde{\rho}^{2}e^{-\frac{\rho^{2}}{2w_{0}^{2}}}e^{-i(k_{e}z-\omega_{c}t)}\hat{\epsilon}_{v}, \\ \vec{E}_{f} &= E_{ef}\frac{1}{50}(-300i\tilde{z}-856i\tilde{z}^{3}-1068\tilde{z}^{4}+468i\tilde{z}^{5}+56\tilde{z}^{6})e^{-\frac{\eta^{2}}{2w_{0}^{2}}}e^{-i(k_{f}y-\omega_{f}t)}\hat{\epsilon}_{v}, \\ \vec{E}_{g} &= E_{gh}\tilde{\rho}^{2}\cos2\phi e^{-\frac{\rho^{2}}{2w_{0}^{2}}}e^{-i(k_{g}z-\omega_{g}t)}\hat{\epsilon}_{v}, \end{split}$$

$$\begin{split} \vec{E}_h &= E_{gh}(224\tilde{z}^2 - 112\tilde{z}^4)e^{-\frac{g^2}{2w_0^2}}e^{-i(k_h y - \omega_h t)}\hat{\epsilon}_v, \\ \vec{E}_i &= E_{ij}\tilde{\rho}^2 \sin 2\phi e^{-\frac{\rho^2}{2w_0^2}}e^{-i(k_i z - \omega_h t)}\hat{\epsilon}_v, \\ \vec{E}_j &= E_{ij}(192\tilde{z} + 192\tilde{z}^3 - 96i\tilde{z}^4)e^{-\frac{g^2}{2w_0^2}}e^{-i(k_j y - \omega_j t)}\hat{\epsilon}_v, \\ \vec{E}_k &= E_{kl}\tilde{\rho}^4 e^{-\frac{\rho^2}{2w_0^2}}e^{-i(k_k z - \omega_k t)}\hat{\epsilon}_v, \\ \vec{E}_l &= E_{kl}(-600i\tilde{z} - 1368\tilde{z}^2 + 936i\tilde{z}^3 + 168\tilde{z}^4)e^{-\frac{g^2}{2w_0^2}}e^{-i(k_l y - \omega_l t)}\hat{\epsilon}_v, \\ \vec{E}_m &= E_{mn}\tilde{\rho}^4 \cos 2\phi e^{-\frac{\rho^2}{2w_0^2}}e^{-i(k_m z - \omega_m t)}\hat{\epsilon}_v, \\ \vec{E}_n &= -E_{mn}224\tilde{z}^2 e^{-\frac{g^2}{2w_0^2}}e^{-i(k_n y - \omega_n t)}\hat{\epsilon}_v, \\ \vec{E}_o &= E_{op}\tilde{\rho}^4 \sin 2\phi e^{-\frac{\rho^2}{2w_0^2}}e^{-i(k_o z + \omega_o t)}\hat{\epsilon}_v, \\ \vec{E}_p &= E_{op}(192\tilde{z} - 192i\tilde{z}^2)e^{-\frac{g^2}{2w_0^2}}e^{-i(k_p y - \omega_p t)}\hat{\epsilon}_v, \\ \vec{E}_q &= E_{qr}\tilde{\rho}^6 e^{-\frac{\rho^2}{2w_0^2}}e^{-i(k_q z - \omega_q t)}\hat{\epsilon}_v, \\ \vec{E}_r &= E_{ar}(312i\tilde{z} + 112\tilde{z}^2)e^{-\frac{g^2}{2w_0^2}}e^{-i(k_r y - \omega_r t)}\hat{\epsilon}_p, \end{split}$$
(A3)

where k_{ζ} with $\zeta = a, b, ..., r$ are angular wave numbers for different laser fields. For both the trefoil and figure-8 knots, the one-photon detunings of the Raman lasers, $\Delta_{\alpha,m_F,m_F'}^{\mathcal{F}}$, with $\alpha=a,b,\ldots,r$, are calculated from the one-photon detunings Δ_{α} , with $\alpha=a,b,\ldots,r$, from the $5S_{\frac{1}{2}}$, F=1, $m_F=0 \to 5P_{\frac{1}{2}}$, F=1, $m_F=0$ transition while taking the proper Zeeman shifts of the energy levels into consideration. Specifically, in our calculation, $\Delta_a = -2\pi \times 236\,\mathrm{MHz}$, $\Delta_b = -2\pi \times 264\,\mathrm{MHz}$, $\Delta_c = -2\pi \times 264\,\mathrm{MHz}$ $-2\pi \times 286\,\mathrm{MHz},\ \Delta_d = -2\pi \times 314\,\mathrm{MHz},\ \Delta_e = -2\pi \times 336\,\mathrm{MHz},\ \Delta_f = -2\pi \times 364\,\mathrm{MHz},\ \Delta_g = -2\pi \times 386\,\mathrm{MHz},\ \Delta_h = -2\pi \times 386\,\mathrm{MHz}$ $-2\pi \times 414 \,\text{MHz}, \ \Delta_i = -2\pi \times 436 \,\text{MHz}, \ \Delta_j = -2\pi \times 464 \,\text{MHz}, \ \Delta_k = -2\pi \times 486 \,\text{MHz}, \ \Delta_l = -2\pi \times 514 \,\text{MHz}, \ \Delta_m = -2\pi \times 414 \,\text{MHz}$ $-2\pi \times 536$ MHz, $\Delta_n = -2\pi \times 564$ MHz, $\Delta_o = -2\pi \times 586$ MHz, $\Delta_p = -2\pi \times 614$ MHz, $\Delta_q = -2\pi \times 636$ MHz, and $\Delta_r = -2\pi \times 664 \,\mathrm{MHz}$, where a negative sign indicates red detuning. All of the laser detunings are achievable with acousto-optical modulators or other devices that can be used to shift the laser frequency. The two-photon detunings between lasers a and b, c and d, e and f, and g and h are all zero. Also, the state independent amplitude of the one-photon Rabi frequencies for imprinting the trefoil knot are $\Omega_{ab}=d_{D_1}E_{ab}/\hbar=2\pi\times795.8\,\mathrm{kHz},~\Omega_{cd}=d_{D_1}E_{cd}/\hbar=100\,\mathrm{kHz}$ $2\pi \times 891.9 \text{ kHz}$, $\Omega_{ef} = d_{D_1} E_{ef}/\hbar = 2\pi \times 984.7 \text{ kHz}$ and $\Omega_{gh} = d_{D_1} E_{gh}/\hbar = 2\pi \times 1075.0 \text{ kHz}$, respectively. The resulting spatially independent amplitude of the two-photon Rabi frequency in Eq. (8) is $\Omega_0 \approx 2\pi \times 162 \,\mathrm{Hz}$, and the largest laser power needed is about 12 mW. For imprinting the figure-8 knot, the one-photon Rabi frequencies in Eq. (A3) are taken as $\Omega_{ab} = d_{D_1} E_{ab}/\hbar = 2\pi \times 159.2 \, \text{kHz}, \, \Omega_{cd} = d_{D_1} E_{cd}/\hbar = 2\pi \times 178.4 \, \text{kHz}, \, \Omega_{ef} = d_{D_1} E_{ef}/\hbar = 2\pi \times 196.9 \, \text{kHz}, \, \Omega_{gh} = 2\pi \times 196.9 \, \text{kHz}$ $d_{D_1}E_{gh}/\hbar = 2\pi \times 215.0 \text{ kHz}, \quad \Omega_{ij} = d_{D_1}E_{ij}/\hbar = 2\pi \times 232.7 \text{ kHz}, \quad \Omega_{kl} = d_{D_1}E_{kl}/\hbar = 2\pi \times 250.1 \text{ kHz}, \quad \Omega_{mn} = d_{D_1}E_{mn}/\hbar = 2\pi \times 250.1 \text{ kHz}, \quad \Omega_{mn} = d_{D_1}E_{mn}/\hbar = 2\pi \times 250.1 \text{ kHz}, \quad \Omega_{mn} = d_{D_1}E_{mn}/\hbar = 2\pi \times 250.1 \text{ kHz}, \quad \Omega_{mn} = d_{D_1}E_{mn}/\hbar = 2\pi \times 250.1 \text{ kHz}, \quad \Omega_{mn} = d_{D_1}E_{mn}/\hbar = 2\pi \times 250.1 \text{ kHz}, \quad \Omega_{mn} = d_{D_1}E_{mn}/\hbar = 2\pi \times 250.1 \text{ kHz}, \quad \Omega_{mn} = d_{D_1}E_{mn}/\hbar = 2\pi \times 250.1 \text{ kHz}, \quad \Omega_{mn} = d_{D_1}E_{mn}/\hbar = 2\pi \times 250.1 \text{ kHz}, \quad \Omega_{mn} = d_{D_1}E_{mn}/\hbar = 2\pi \times 250.1 \text{ kHz}, \quad \Omega_{mn} = d_{D_1}E_{mn}/\hbar = 2\pi \times 250.1 \text{ kHz}, \quad \Omega_{mn} = d_{D_1}E_{mn}/\hbar = 2\pi \times 250.1 \text{ kHz}, \quad \Omega_{mn} = d_{D_1}E_{mn}/\hbar = 2\pi \times 250.1 \text{ kHz}, \quad \Omega_{mn} = d_{D_1}E_{mn}/\hbar = 2\pi \times 250.1 \text{ kHz}, \quad \Omega_{mn} = d_{D_1}E_{mn}/\hbar = 2\pi \times 250.1 \text{ kHz}, \quad \Omega_{mn} = d_{D_1}E_{mn}/\hbar = 2\pi \times 250.1 \text{ kHz}, \quad \Omega_{mn} = d_{D_1}E_{mn}/\hbar = 2\pi \times 250.1 \text{ kHz}, \quad \Omega_{mn} = d_{D_1}E_{mn}/\hbar = 2\pi \times 250.1 \text{ kHz}, \quad \Omega_{mn} = d_{D_1}E_{mn}/\hbar = 2\pi \times 250.1 \text{ kHz}, \quad \Omega_{mn} = d_{D_1}E_{mn}/\hbar = 2\pi \times 250.1 \text{ kHz}, \quad \Omega_{mn} = d_{D_1}E_{mn}/\hbar = 2\pi \times 250.1 \text{ kHz}, \quad \Omega_{mn} = d_{D_1}E_{mn}/\hbar = 2\pi \times 250.1 \text{ kHz}, \quad \Omega_{mn} = d_{D_1}E_{mn}/\hbar = 2\pi \times 250.1 \text{ kHz}, \quad \Omega_{mn} = d_{D_1}E_{mn}/\hbar = 2\pi \times 250.1 \text{ kHz}, \quad \Omega_{mn} = d_{D_1}E_{mn}/\hbar = 2\pi \times 250.1 \text{ kHz}, \quad \Omega_{mn} = d_{D_1}E_{mn}/\hbar = 2\pi \times 250.1 \text{ kHz}, \quad \Omega_{mn} = d_{D_1}E_{mn}/\hbar = 2\pi \times 250.1 \text{ kHz}, \quad \Omega_{mn} = d_{D_1}E_{mn}/\hbar = 2\pi \times 250.1 \text{ kHz}, \quad \Omega_{mn} = d_{D_1}E_{mn}/\hbar = 2\pi \times 250.1 \text{ kHz}, \quad \Omega_{mn} = d_{D_1}E_{mn}/\hbar = 2\pi \times 250.1 \text{ kHz}, \quad \Omega_{mn} = d_{D_1}E_{mn}/\hbar = 2\pi \times 250.1 \text{ kHz}, \quad \Omega_{mn} = d_{D_1}E_{mn}/\hbar = 2\pi \times 250.1 \text{ kHz}, \quad \Omega_{mn} = d_{D_1}E_{mn}/\hbar = 2\pi \times 250.1 \text{ kHz}, \quad \Omega_{mn} = d_{D_1}E_{mn}/\hbar = 2\pi \times 250.1 \text{ kHz}, \quad \Omega_{mn} = d_{D_1}E_{mn}/\hbar = 2\pi \times 250.1 \text{ kHz}, \quad \Omega_{mn} = d_{D_1}E_{mn}/\hbar = 2\pi \times 250.1 \text{ kHz}, \quad \Omega_{mn} = d_{D_1}E_{mn}/\hbar = 2\pi \times 250.1 \text{ kHz}, \quad \Omega_{mn} = d_{D_1}E_{mn}/\hbar = 2\pi \times 250.1 \text{ kHz}, \quad \Omega_{mn} = d_{D_1}E_{mn}/\hbar = 2\pi \times 250.1 \text{ kHz}, \quad \Omega_{mn} = d_{D_1}E_{mn}/\hbar = 2\pi \times 250.1 \text{ kHz$ $2\pi \times 267.2$ kHz, $\Omega_{op} = d_{D_1} E_{op}/\hbar = 2\pi \times 284.2$ kHz, and $\Omega_{qr} = d_{D_1} E_{qr}/\hbar = 2\pi \times 300.9$ kHz, respectively. The resulting spatially independent amplitude of the two-photon Rabi frequency in Eq. (A2) is $\Omega_0 \approx 2\pi \times 65$ Hz, and the largest laser power needed is about 300 mW. To optimize the laser power and spatial profile, one could apply the optical field optimization algorithm in Ref. [14]. Also, one could reduce the laser powers of the topologically nontrivial Raman lasers and increase the power of Gaussian lasers. The undesired, spatially varying AC Stark shifts could be canceled optically [37], or with magnetic fields [38,39]. In all the one-photon Rabi frequencies above, \vec{d}_{D_1} denotes the electric dipole moment of the ⁸⁷Rb D_1 transition. The bias magnetic field is taken to be $B = 20 \,\mathrm{G}$.

C. F. Barenghi, Knots and unknots in superfluid turbulence, Milan J. Math. 75, 177 (2007).

^[2] R. G. Cooper, M. Mesgarnezhad, A. W. Baggaley, and C. F. Barenghi, Knot spectrum of turbulence, Sci. Rep. 9, 10545

^[3] D. Proment, M. Onorato, and C. F. Barenghi, Vortex knots in a Bose-Einstein condensate, Phys. Rev. E **85**, 036306 (2012).

^[4] D.-L. Deng, S.-T. Wang, K. Sun, and L.-M. Duan, Probe knots and Hopf insulators with ultracold atoms, Chin. Phys. Lett. 35, 013701 (2017).

^[5] W.-K. Bai, T. Yang, and W.-M. Liu, Topological transition from superfluid vortex rings to isolated knots and links, Phys. Rev. A 102, 063318 (2020).

^[6] D.-L. Deng, S.-T. Wang, C. Shen, and L.-M. Duan, Hopf insulators and their topologically protected surface states, Phys. Rev. B 88, 201105(R) (2013).

^[7] P. Sutcliffe, Skyrmion Knots in Frustrated Magnets, Phys. Rev. Lett. **118**, 247203 (2017).

^[8] D. Kleckner and W. T. Irvine, Creation and dynamics of knotted vortices, Nat. Phys. 9, 253 (2013).

- [9] W. R. Taylor, A deeply knotted protein structure and how it might fold, Nature (London) 406, 916 (2000).
- [10] D. Han, S. Pal, Y. Liu, and H. Yan, Folding and cutting DNA into reconfigurable topological nanostructures, Nat. Nanotechnol. 5, 712 (2010).
- [11] A. Suma and C. Micheletti, Pore translocation of knotted DNA rings, Proc. Natl. Acad. Sci. USA 114, E2991 (2017).
- [12] T. Chen, X. Zheng, Q. Pei, D. Zou, H. Sun, and X. Zhang, Creation of electrical knots and observation of DNA topology, New J. Phys. 23, 093045 (2021).
- [13] H. Larocque, A. D'Errico, M. F. Ferrer-Garcia, A. Carmi, E. Cohen, and E. Karimi, Optical framed knots as information carriers, Nat. Commun. 11, 5119 (2020).
- [14] M. R. Dennis, R. P. King, B. Jack, K. O'holleran, and M. J. Padgett, Isolated optical vortex knots, Nat. Phys. 6, 118 (2010)
- [15] D. Sugic and M. R. Dennis, Singular knot bundle in light, J. Opt. Soc. Am. A 35, 1987 (2018).
- [16] B. Bode, M. R. Dennis, D. Foster, and R. P. King, Knotted fields and explicit fibrations for lemniscate knots, Proc. R. Soc. A 473, 20160829 (2017).
- [17] H. Larocque, D. Sugic, D. Mortimer, A. J. Taylor, R. Fickler, R. W. Boyd, M. R. Dennis, and E. Karimi, Reconstructing the topology of optical polarization knots, Nat. Phys. 14, 1079 (2018).
- [18] L. S. Leslie, A. Hansen, K. C. Wright, B. M. Deutsch, and N. P. Bigelow, Creation and Detection of Skyrmions in a Bose-Einstein Condensate, Phys. Rev. Lett. 103, 250401 (2009).
- [19] J. T. Schultz, A. Hansen, J. D. Murphree, M. Jayaseelan, and N. P. Bigelow, Creating full-Bloch Bose–Einstein condensates with Raman q-plates, J. Opt. 18, 064009 (2016).
- [20] A. Hansen, J. T. Schultz, and N. P. Bigelow, Singular atom optics with spinor Bose-Einstein condensates, Optica 3, 355 (2016).
- [21] W. Lee, A. H. Gheorghe, K. Tiurev, T. Ollikainen, M. Möttönen, and D. S. Hall, Synthetic electromagnetic knot in a three-dimensional skyrmion, Sci. Adv. 4, eaao3820 (2018).
- [22] Y. Kawaguchi, M. Nitta, and M. Ueda, Knots in a Spinor Bose-Einstein Condensate, Phys. Rev. Lett. **100**, 180403 (2008).
- [23] D. S. Hall, M. W. Ray, K. Tiurev, E. Ruokokoski, A. H. Gheorghe, and M. Möttönen, Tying quantum knots, Nat. Phys. 12, 478 (2016).
- [24] T. Ollikainen, A. Blinova, M. Möttönen, and D. S. Hall, Decay of a Quantum Knot, Phys. Rev. Lett. 123, 163003 (2019).

- [25] C. W. Duncan, C. Ross, N. Westerberg, M. Valiente, B. J. Schroers, and P. Öhberg, Linked and knotted synthetic magnetic fields, Phys. Rev. A 99, 063613 (2019).
- [26] J. Ruostekoski and Z. Dutton, Engineering vortex rings and systems for controlled studies of vortex interactions in Bose-Einstein condensates, Phys. Rev. A 72, 063626 (2005).
- [27] F. Maucher, S. Gardiner, and I. Hughes, Excitation of knotted vortex lines in matter waves, New J. Phys. 18, 063016 (2016).
- [28] K. Brauner, Das verhalten der funktionen in der umgebung ihrer verzweigungsstellen, in Abhandlungen aus dem Mathematischen Seminar der Universität Hamburg (Springer, Berlin, 1928), Vol. 6, pp. 1–55.
- [29] R. P. King, Knotting of optical vortices, Ph.D. thesis, University of Southampton, 2010.
- [30] C. Cohen-Tannoudji, J. Dupont-Roc, and G. Grynberg, *Atom-Photon Interactions: Basic Processes and Applications* (Wiley-VCH, Berlin, 1998).
- [31] K. C. Wright, L. S. Leslie, and N. P. Bigelow, Raman coupling of Zeeman sublevels in an alkali-metal Bose-Einstein condensate, Phys. Rev. A **78**, 053412 (2008).
- [32] D. A. Steck, Rubidium 87 d line data (2001).
- [33] V. Lerner, D. Shwa, Y. Drori, and N. Katz, Shaping Laguerre-Gaussian laser modes with binary gratings using a digital micromirror device, Opt. Lett. 37, 4826 (2012).
- [34] Y.-X. Ren, Z.-X. Fang, L. Gong, K. Huang, Y. Chen, and R.-D. Lu, Digital generation and control of Hermite-Gaussian modes with an amplitude digital micromirror device, J. Opt. 17, 125604 (2015).
- [35] J. T. Schultz, Singular atom optics via stimulated Raman interactions in Spinor Bose-Einstein condensates, Ph.D. thesis, University of Rochester, 2016.
- [36] A. Hansen, Topological spin textures in Spinor Bose-Einstein condensates generated by stimulated Raman interactions, Ph.D. thesis, University of Rochester, 2016.
- [37] Z. Chen, H. Yao, E. Haber, and N. P. Bigelow, Momentum dependent optical lattice induced by an artificial gauge potential, Phys. Rev. Res. 4, 013124 (2022).
- [38] P. Treutlein, T. W. Hänsch, J. Reichel, A. Negretti, M. A. Cirone, and T. Calarco, Microwave potentials and optimal control for robust quantum gates on an atom chip, Phys. Rev. A 74, 022312 (2006).
- [39] M. Singh, M. Volk, A. Akulshin, A. Sidorov, R. McLean, and P. Hannaford, One-dimensional lattice of permanent magnetic microtraps for ultracold atoms on an atom chip, J. Phys. B: At. Mol. Opt. Phys. 41, 065301 (2008).